Experiments and modeling of an instability of an atmospheric pressure arc

Max Karasik[a] and S. J. Zweben
Princeton Plasma Physics Laboratory, P.O. Box 451, Princeton, New Jersey 08543

(Received 30 November 1999; accepted 13 June 2000)

An instability of a free-burning atmospheric pressure ≈200 A carbon arc is investigated experimentally and modeled analytically. The presence of the instability is found to depend critically on cathode dimensions. In particular, for cylindrical cathodes, the instability occurs only for a narrow range of cathode diameters. Cathode spot motion is proposed as the mechanism of the instability. A simple fluid model combining the effect of the cathode spot motion and the inertia of the cathode jet successfully describes the shape of the arc column during low amplitude instability. The amplitude of cathode spot motion required by the model is in agreement with measurements. The average jet velocity required is approximately equal to that found from applied oscillating transverse magnetic field experiments. The primary reasons for cathode spot motion are most likely cathode vaporization and interaction of arc current with the current distribution in the cathode. Cathode surface temperature distribution is likely to be the reason for cathode geometry dependence. © *2000 American Institute of Physics.* [S1070-664X(00)00310-4]

I. INTRODUCTION

Atmospheric pressure arcs have numerous applications in materials processing,[1] metallurgy,[2] and welding.[3] In many cases, arc instabilities are deleterious to device performance, resulting in, for example, voltage fluctuations that can propagate onto the electric power grid.[4,5] Moreover, arc instabilities can cause arc extinctions and can limit the length of arc that can be sustained in a particular device.

Our previous paper[6] dealt with driven regular motion of a stable arc under the influence of an applied magnetic field. The present work gives a description and analysis of unstable arc behavior of the same arc observed under certain conditions with no external applied magnetic field.

We use the term ''instability'' to describe the observed spontaneous arc motion with strong fluctuations in position, current, and voltage. We believe that this is not an instability of the arc column *per se*, but rather an instability of the cathode attachment spot which causes the arc to move. This motion is sometimes periodic and sometimes turbulent, particularly at large amplitude. An audible sound is produced during the instability. The phenomenology of the instability and the specific conditions under which it occurs are described in Sec. III.

The organization of this paper is as follows: First, an overview of previous work is given, the experimental setup is described in Sec. II, the experimental results are given in Sec. III, a model for the instability is developed and applied to the experimental data in Sec. IV, and cathode processes affecting arc stability are discussed in Sec. V. Last, a discussion of the results and conclusions are given in Sec. VI.

A. An overview of previous work

The literature contains several cases of direct comparisons between theories of arc instabilities and experiments. All of these cases, however, involve low intensity arcs, with currents of order ~10 A, where electrode jet effects are insignificant. Hülsmann and Mentel[7,8] have done a comprehensive study of the stability of a low current (~10 A), long, wall-stabilized atmospheric pressure hydrogen arc. Gaede[9] investigated a free-burning ~10 A hydrogen arc with one end fixed by a diaphragm and the other free to move in a plane.

Ragaller[10] derives the functional form of linear stability behavior of an infinitely long arc column against the $m=1$ kink mode with the aid of dimensional analysis. Stability was determined by the balance of the self-magnetic field of the helically disturbed column and asymmetrical heating effects. It was assumed that axial flow effects can be treated by choosing a reference frame moving with the flow, and are not included in the treatment. It is mentioned, however, that the flow can stabilize the arc if the instability growth rate is slow enough.

A helical instability of a wall-stabilized hydrogen arc burning in a 3-mm-diam tube at 500–900 Torr pressures and currents up to 120 A was studied experimentally in Ref. 11. The onset of the instability was explained on the basis of the competition between the destabilizing self-magnetic forces and the stabilizing effect of the wall and inhomogeneous heat flow tending to straighten the current path.

Several investigations had focused on the stability of high-current arcs in an imposed accelerating flow, such as found in gas-blast circuit breakers and arc heaters. In Ref. 12, a numerical study of such an arrangement finds instability due to shear flow amplification of density fluctuations. In Ref. 13, an experimental investigation of a 20–500 A ac arc in accelerating flow revealed similarities with the instabilities seen in fluid jets. The work concludes that the instabilities arose from the shear layers between the cold gas flow and the more accelerated plasma of the arc column. Reference 14 describes experiments on a nitrogen arc in accelerating flow at 25 atm. The helical instability observed was analyzed on

[a]Present address: Naval Research Lab, Code 6731, 4555 Overlook Ave. SW, Washington, DC 20375; electronic mail: karasik@this.nrl.navy.mil

the basis of destabilizing self-magnetic forces and convective stabilization by the imposed flow.

Bellan *et al.*[15] performed experiments on arc instability initiated by a transverse magnetic field on a pulsed, ≈ 1 kA, 0.6-cm-long arc. The instability was treated as being driven by the self-magnetic field of the arc and the centrifugal force of the cathode jet flow. Stabilization of the arc blowout was accomplished with an external axial magnetic field on the order of the self-field of the arc. However, the axial field was also found to induce helical rotation of the arc column.

Voltage fluctuations on a 2 kA ac experimental arc furnace were analyzed for deterministic chaos in Ref. 16. It was found that the fluctuations are indicative of a low dimensional chaotic system. The paper further suggests that real-time control of the fluctuations may be possible.

Alternating current (ac) arcs with a geometry similar to the present experiments (free burning between a graphite rod and a steel plate), but at an order of magnitude higher currents (≈ 10 kA ac) were observed by Bowman and Jordan.[17] The arc was observed to be stable during the half-cycle with the graphite as cathode (the case in the present experiments), and contorted by ''kinks'' when the graphite was the anode. A strong cathode jet was present during the former, and absent in the latter. The stability in the former case was explained by the stabilizing effect of the cathode jet momentum, which precluded self-magnetic ''kinking'' for short wavelengths. It was concluded that the arc was stable in this case because the estimated minimum wavelength for instability was longer than the arc length.

The instability studied in the present work is first mentioned in Ref. 18 for free-burning arcs between graphite electrodes for currents greater than 400 A. Witkowski[19] investigated this instability experimentally and suggested a fire-hose-type instability mechanism. Montgomery and Sharp[20] observed the instability for an arc between ~ 5-cm-diam graphite rod cathodes and a graphite plate anode in the range of 400–2000 A. It was found that the current threshold for the instability depended on the geometry of the cathode tip: the arc was stabilized by the presence of a sharp edge on the cathode, and became unstable as soon as the edge was eroded. It was suggested that this dependence is a result of the influence of the current distribution in the cathode on arc stability.

A recent theoretical work[21] examined arc stability in an external axial magnetic field. Instability was studied for an infinitely long arc column on time scales slower than the resistive and viscous diffusion time scales. It was concluded that the arc is unstable to helical perturbations with wavelengths on the order of $2\pi \times$(arc radius) with the axial magnetic field, and marginally stable to such perturbations with no external magnetic field applied. The analysis was performed without any zero-order flows, such as cathode jets.

In summary, detailed experimental and theoretical analysis of arc column instabilities is found in the literature for low current ($\leqslant 100$ A) arcs.[7–9] For such arcs, the destabilizing mechanism is usually found to be a magnetic ''kink.'' Experimental studies usually aim to minimize the influence of the electrodes on the discharge and theoretical analysis tends to disregard their effects.[21,10]

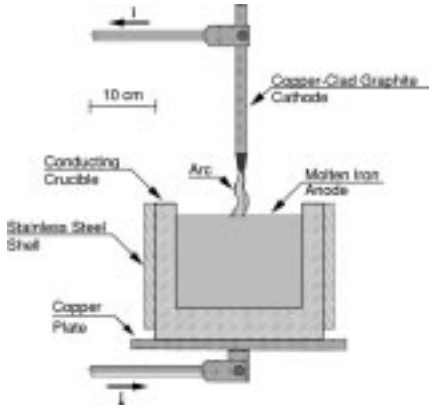

FIG. 1. Experimental setup (side view). Shown is the iron anode in the MgO conducting crucible.

Experiments and analysis is scarce for free-burning higher-current arcs. There are conflicting conclusions as to the stabilizing or destabilizing role of the cathode jet (e.g., Bowman[17] versus Bellan[15]). Cathode geometry effect is found to be critical to stability.[20] However, no satisfactory explanation of the effect is found.

Experimental studies of industrial scale arcs (~ 100 kA) are based on limited visual observations of instabilities, with analysis usually highly speculative, consisting mostly of extrapolations from lower currents or from fluid mechanic phenomena.[2] However, it is clear that such arcs are almost always highly unstable.[2,22]

II. EXPERIMENTAL SETUP

The apparatus used in the instability study is the same as in Ref. 6 with the exception of the lack of an applied transverse magnetic field. A schematic of the apparatus is shown in Fig. 1. The arc is struck by contact between a vertical graphite rod cathode and a flat metal surface anode whose diameter is much larger than the arc diameter. The electrode gap is adjustable in the range 0–7 cm by moving the cathode. The arc is burning at atmospheric pressure in air. Power is supplied from a current-regulated (on the 60 Hz time scale) 30 kW dc power supply via a noninductive 0.12 Ω ballast resistor in series with the arc.

The same type of instability has been observed with both an iron anode in the MgO crucible as well as with nonmagnetic stainless steel anodes. However, all of the quantitative analysis presented in the following is for stainless steel anodes. Additionally, in order to determine the effect of cathode geometry on arc stability, cathodes of various tip diameters and tip shapes are utilized.

The shape of the arc is obtained using an intensified charge coupled device camera (ITT 4577) with typically a 10 μs gate duration at a rate of 60 frames/s. A polished steel mirror is used to capture a 90° view of the arc in each frame in addition to the direct view. The raw image of the arc as captured by a frame grabber is processed to give the coordinates of the points along the center of the luminous arc col-

umn by finding the centroid of brightness along each horizontal line of pixels. The arc shape is defined as the locus of such points.

Continuous monitoring of the arc column position along a horizontal line is accomplished using a linear array of eight collimated photodiodes with a bandwidth of 80 kHz. Data acquisition is synchronized to the gating pulse of the camera. A more detailed description of the setup and diagnostics is given in Ref. 23.

A typical ''run'' is done as follows. A particular kind of cathode to be studied is installed on the apparatus. The cathode is lowered to contact the anode. The current is raised to 150 A. The cathode is raised approximately 1 cm from the anode, drawing an arc. Approximately 30 s is allowed before data taking for the anode surface to melt. The experiments are carried out for 5–10 min, at variable currents and electrode gaps, until the anode as a whole becomes too hot (side surface temperature $\approx 500\,^{\circ}\mathrm{C}$). If the arc extinguishes during the run, it is restarted by bringing the cathode back in contact with the anode and separating them as before. Each data acquisition sample consists of 0.5 s (30 fields) of image acquisition and 3.3 s fast acquisition of the current, voltage, and photodiode wave forms, synchronized to the camera gating. Typically, 20–30 such samples are collected per 5–10 min run.

A stable arc typically has less than 1% rms current fluctuation and is burning vertically on the electrode axis except for a slow precession (≈ 20 s period) around the cathode tip. The direction of the precession can be either clockwise or counterclockwise and can switch while the arc is burning. The origin of this precession is discussed in Sec. V B 2.

III. EXPERIMENTAL RESULTS

The instability occurs with no externally applied magnetic field. During the instability, the arc column develops a three-dimensional (3-D) wriggling helical shape, with the amplitude of the helix increasing toward the anode. Both left- and right-handed helixes are observed. The arc moves continuously on the anode surface; cathode spot motion has also been observed during many unstable runs. A series of pictures of the arc taken using the gated camera during typical unstable behavior is shown in Fig. 2. For comparison, views of a stable arc are also shown at the top.

A. Overview of the instability

The instability is accompanied by typically up to $\approx 10\%$ rms current fluctuations and $\approx 5\%$ rms voltage fluctuations. A plot of the current fluctuation amplitude in the (electrode gap versus arc current) parameter space for a set of runs is shown in Fig. 3. As can be seen in the figure, the fluctuation level increases with current and electrode gap. For the standard 3/8 in. cathode, no instability has been observed below 120 A. Also, although the amplitude of the voltage and current oscillation for unstable arc increases with electrode gap, the electrode gap, and therefore the arc length, does not affect the current threshold of the instability.

The arc instability has been found at all arc lengths in the range 1–7 cm. For short arcs in the range of 1–2 cm, especially when the fluctuation frequency is low, the arc column is deformed by only a fraction of a wavelength, and its motion as a whole along the cathode surface is apparent. Below approximately 0.5 cm, the proximity of electrodes and the interaction of anode vapors and the impinging cathode jet can produce erratic arc motion regardless of whether the arc was stable at longer gaps.

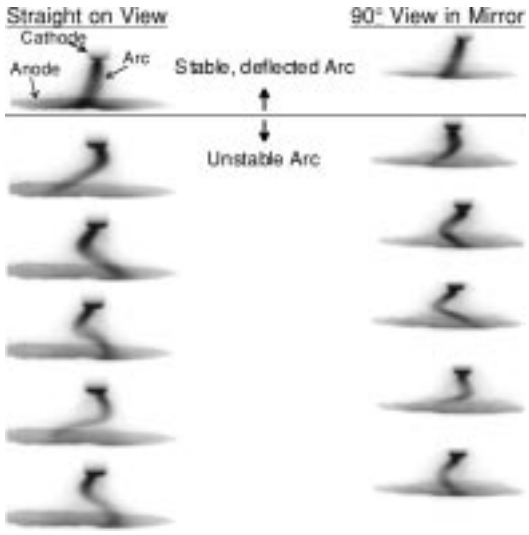

FIG. 2. Sample images of unstable arc during low amplitude oscillation. The left-hand column shows the direct view of the arc; the right-hand column shows a 90° view in the mirror. The horizontal scale is expanded 2.4:1 in direct view and 2.3:1 in the mirror view. The cathode–anode gap is 3.1 cm. The five unstable arc frames were picked from a 30 frame data sample to illustrate different arc column shapes.

The frequency range of the current and voltage fluctuations is approximately 200–1000 Hz. A whistling sound is heard during many of the instability runs, as the frequency range is in the audio frequencies. For low amplitudes, the arc current fluctuation spectrum typically consists of strong

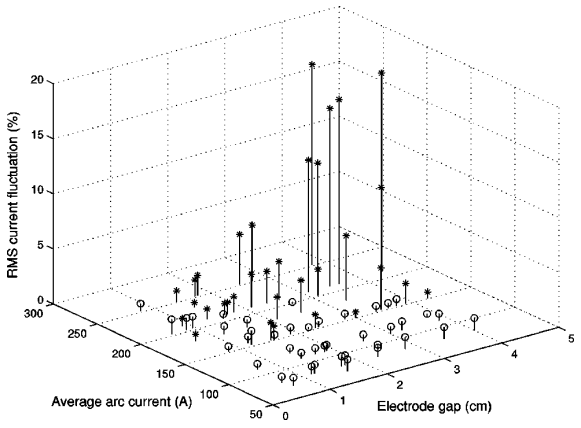

FIG. 3. Measured rms current fluctuation vs current and electrode gap for a standard 3/8 in. cathode. Stable runs are marked with an open circle, unstable with an asterisk. The fluctuation level increases with current and electrode gap. For a stable arc, the fluctuation level is typically $<1\%$.

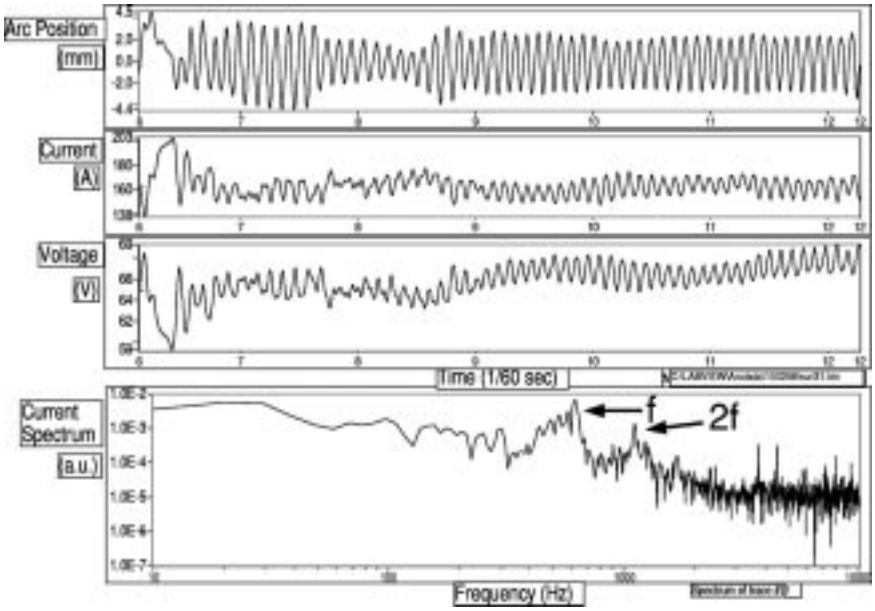

FIG. 4. Wave forms of a typical low amplitude unstable run. Arc position refers to the center of a horizontal cross section of the arc at a fixed distance above the anode, and is varying at ≈ 600 Hz. A$\approx$1200 Hz harmonic is prominent on the current spectrum in addition to the fundamental. In this and all the following wave form figures, the time scale is marked in fields taken by the gated camera at 59.939 fields per second, i.e., one unit on the time scale $\approx$1/60 s. 0 on the time scale corresponds to the gate of the first field taken by the camera, 1 to the second, and so on. The current spectra are the amplitude of the fast Fourier transforms of the arc current over the time interval displayed.

peaks at a fundamental and a harmonic, with higher harmonics present during some runs. Typical wave forms and spectrum for the instability at low amplitude are shown in Fig. 4. The peak frequencies vary by approximately 10% during a 3 s data acquisition sample. The relative strength of the fundamental and its harmonic on the voltage and current varies and either one can be dominant. The presence of the harmonic is expected from the model of the instability presented in Sec. IV, since, as shown in Ref. 23, the model predicts arc length variation at twice the column oscillation frequency.

Another feature seen in Fig. 4 is that the current and voltage fluctuations are 180° out of phase with each other, with the current to voltage amplitude ratio of 0.13. The same was found for a stable arc in an applied ac transverse magnetic field.[6] This relationship is discussed in detail in Ref. 23 and is found to be due to a large (0.21 F) capacitor internal to the arc power supply across its output and the presence of a $0.12 \pm 0.01\ \Omega$ ballast resistor in series. The voltage across the arc, V_{arc}, and the voltage across the power supply, V_s, are related as

$$V_{\mathrm{arc}} = V_s - IR. \tag{1}$$

On the time scale shorter than the RC time of the capacitor and the arc load,

$$\tau = RC = (60\ \mathrm{V}/200\ \mathrm{A})(0.21\ \mathrm{F}) = (0.3\ \Omega)(0.21\ \mathrm{F}) \approx 60\ \mathrm{ms}, \tag{2}$$

the voltage across the capacitor, and therefore, at the output of the power supply, remains constant ($V_s = \mathrm{const}$). Fast fluctuations are thus expected to be related as $\Delta V_{\mathrm{arc}}/\Delta I = -R = -0.12 \pm 0.01\ \Omega$, as seen in the experiments.

The frequency of arc column motion coincides with the fundamental frequency on the current and voltage wave forms. This was ascertained by inferring the column position along a horizontal line from the collimated photodiode array.[23] The inferred column position is also shown as a trace in Fig. 4. The frequency is independent of the electrode gap and increases with arc current.[23] The latter is consistent with the observations of Witkowski,[19] which show the frequency increasing in the range 100–300 A and leveling off for 300–800 A.

Instability onset can be gradual—it does not seem to require a finite ''kick'' for initiation. Fig. 5 shows an example of such a gradual buildup of the oscillation, first in the column motion, then in the voltage and current wave forms. The presence of the instability of the column motion prior to the oscillation developing on the current also indicates that a current oscillation is not part of the mechanism of the instability, at least at low amplitudes.

Instability at low amplitude can be intermittent, occurring in bursts that last from several to thousands of oscillation periods. Moreover, even at higher currents (>180 A), the arc can remain stable for up to a minute or more after its initiation before the instability sets in. Once unstable bursts start to appear, the amplitude of the oscillation and the duration of the bursts typically increase over time, until the arc is wriggling continuously with such a large amplitude that it often leads to arc extinction. The time scale for this development is tens of seconds.

For large amplitude instability, the spectrum no longer has distinguishable peaks, but is broad with a power law characteristic, as shown in Fig. 6.

The shape of the arc column during instability is not always a three-dimensional helix: There are instances when the arc column is wriggling in a plane (see Fig. 7).

In some runs, the arc became stable after a long period of instability. In these cases and others it is found that by bringing the cathode back in contact or close proximity with the anode while the arc is on, then separating the two, insta-

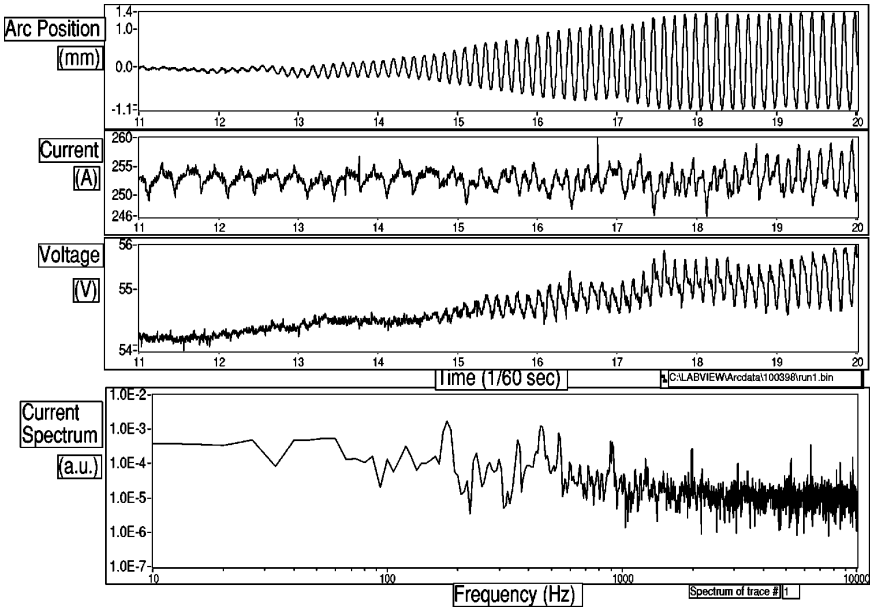

FIG. 5. The onset of the instability can be gradual. The column begins oscillating (''arc position'' trace) before the oscillation shows up on the voltage and current traces. The 180 Hz signal on the current trace noticeable prior to the instability onset is associated with the power supply silicon controlled rectifiers.

bility can be restored. This is apparently due to a dependence on the cathode geometry, discussed in the following.

B. Cathode geometry dependence

It was found that the geometry of the cathode tip plays a crucial role in the arc stability. The dimensions of the many different cathodes used are given in Ref. 23. The effect of the cathode dimensions on stability is summarized in Fig. 8 by a plot of occurrence of instability against the area of the cathode tip. As can be seen in Fig. 8, for solid cylindrical cathode tips, the arc is unstable only in the range of 20–28 mm^2 for the range of currents studied.

The cathode diameter dependence of the instability is dramatically demonstrated by the experiment with the ''necked'' cathode. This cathode had two narrow ''necks'' machined in it with a diameter smaller than the lower stability threshold. The arc was unstable after approximately 15 s of burning on the large area tip, stable while burning through the lower ''neck,'' unstable on the middle button after the lower neck had eroded, stable again on the upper ''neck,'' and became unstable again after reaching the main body of the electrode. Sample images from this sequence are shown in Fig. 9. The arc current was kept constant throughout. Although the arc length was changing as the cathode was eroding, it was probably not a factor, since the change from stability to instability and vice versa occurred at the point where the cathode diameter change occurred. Furthermore, the arclength has not been found to affect the threshold of the instability, as mentioned in Sec. III A.

Besides illustrating the contrast in stability between the narrow and wide sections, the ''necked'' cathode run also exhibited instability on a wider than usual cathode tip when

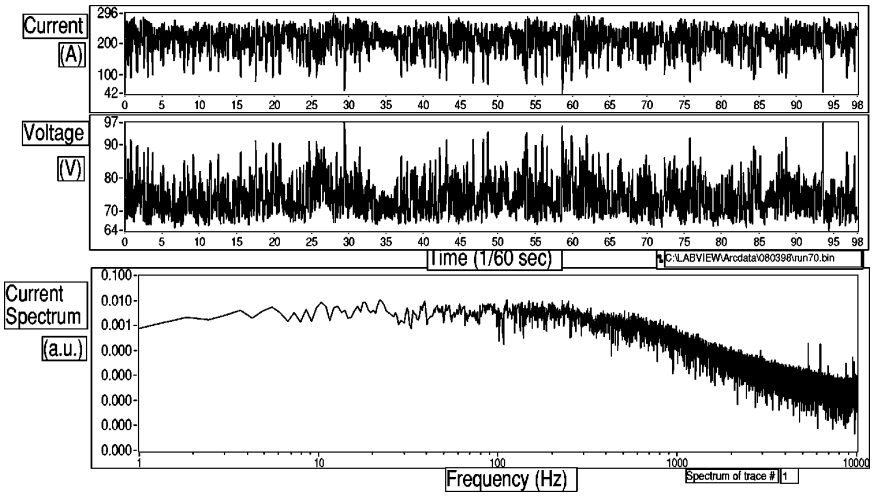

FIG. 6. Wave forms during a large amplitude instability. Note that the wave forms are no longer simple oscillations, and the current spectrum is broad, with a power law decay (≈ 2.9 power). Average arc current is 211 A, with 16% rms fluctuation amplitude.

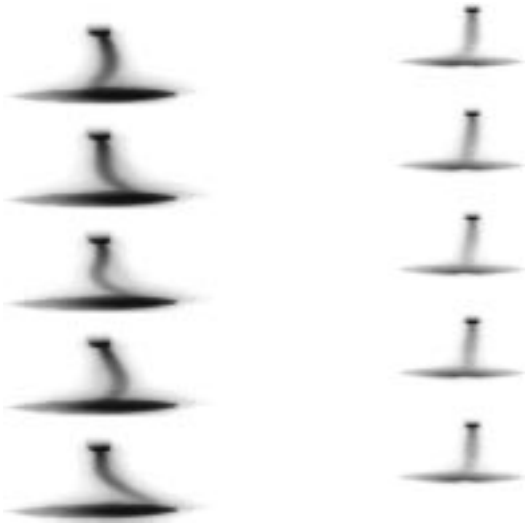

FIG. 7. The instability is not always three dimensional. Here the arc is moving in the direct view (left-hand column) and is stationary in the mirror view (right-hand column). The cathode is a 3/8-in.-diam cylindrical rod.

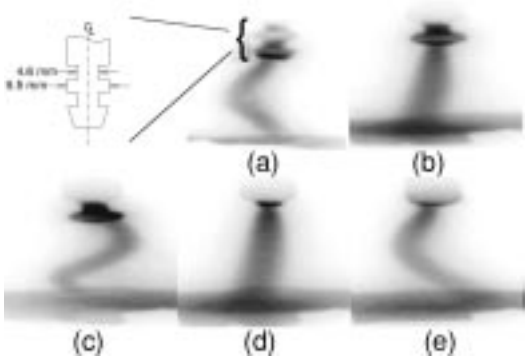

FIG. 9. A time sequence of sample images from the experiment with the ''necked'' cathode (the initial cathode shape is shown schematically). As the cathode is eroding, the arc is (a) unstable on the lower wide section; (b) stable while attached to the remaining part of the lower narrow section; (c) unstable on the middle wide section; (d) stable while burning through the upper narrow section; (e) unstable after the upper narrow neck has been eroded and the main body of the cathode has been reached. Arc current is 250 A. The image in (a) is in the mirror view, (b)–(e) are direct view. The horizontal scale is expanded 2.4:1.

the arc was attached to the middle section [Fig. 9(c)]. The diameter of that section was approximately 8 mm at that time, giving a tip area of ≈ 50 m^2, or about twice as large in area as the upper stability threshold for solid cylindrical cathodes. This is most likely due to its higher than normal temperature for cathodes of this size, as will be discussed further in Sec. V A.

The geometry of the cathode not only affects the threshold for the instability, but also influences the unstable arc shape. An example of the latter is given in Fig. 10, which shows images of instability with a ''paddle'' shaped cathode (8.8 mm wide by 2.5 mm thick; schematic shown in Fig. 10). The amplitude of arc column displacement is significantly greater in the plane of the wide cathode dimension.

C. Cathode spot motion

Cathode spot motion has been observed in many unstable runs. For example, Fig. 10 clearly shows motion of the arc attachment on the cathode. In order to better examine this effect, a series of runs were taken with a close-up view of the cathode region, at approximately 4× the spatial resolution of the standard images.

Fig. 11 shows such close-up images of the cathode region of arc during large amplitude instability. Shown are single exposure as well as double-exposure images. Motion of the point of attachment at the cathode is clearly visible. The double-exposure images, with exposures separated by 2 ms, show that the cathode spot moved on the time scale of the instability ($\approx 1-4$ ms).

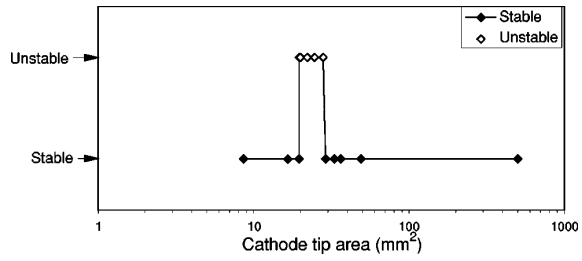

FIG. 8. Arc stability vs the cathode tip area for cylindrical cathodes for currents up to approximately 250 A. The arc is unstable only in the range of 20–28 mm^2.

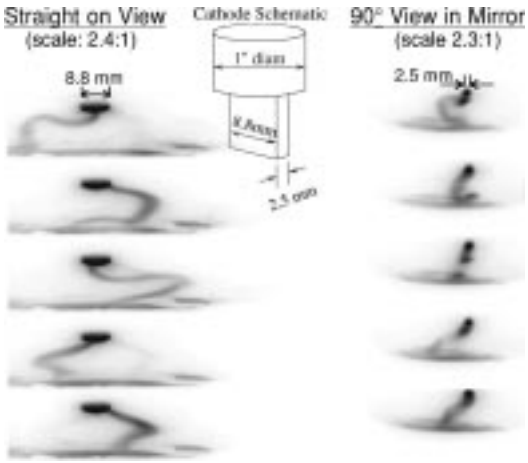

FIG. 10. Sample pictures of unstable arc during large amplitude oscillation on a ''paddle''-shaped cathode (8.8 mm wide by 2.5 mm thick; schematic shown). The left-hand column shows the direct view of the arc; the right-hand column—a 90° view in the mirror. The horizontal scale is expanded. The electrode gap is 2.7 cm. Note that the cathode is wider in the direct view plane and that the amplitude of motion of the arc is greater in that plane. Also notable is that the arc attachment is moving along the tip of the cathode.

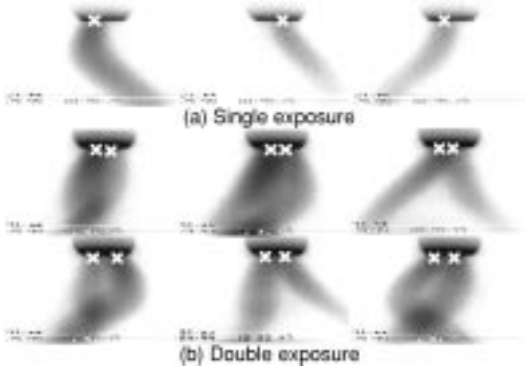

FIG. 11. Close-up images of the cathode region of the arc during large amplitude instability clearly show motion of the arc along the cathode surface (spot motion). A cross marks the approximate cathode spot location. (a) Three fields with a single 5 μs exposure; (b) six fields with two 5 μs exposures per field, with exposures separated by 2 ms. In (b), the two images of the arc column do not overlap completely at the cathode, indicating displacement of the attachment point during the 2 ms between exposures. Arc current is 250 A. The horizontal scale is expanded 2.3:1.

IV. MODEL OF THE INSTABILITY

This section develops a theoretical description of the mechanisms responsible for the instability phenomena described previously. A model of the instability derived in Sec. IV B is applied to the experimental observations in Sec. IV C.

A. Mechanism of the instability

In attempting to discover the mechanism of the instability, several different categories of instabilities have to be considered. Several possible candidates are listed in the following, together with a discussion of their relevance to the observations.

(1) *Electrical circuit oscillation.* Circuit oscillations alone could not account for the three-dimensional displacement of the arc column or the observed dependence of the instability on the cathode geometry. Moreover, as discussed in Sec. III A, arc column oscillation can appear prior to any oscillation of the current or voltage.
(2) *Shear flow.* Instability driven by the shear flows in the jet.[24,25] This type of instability does not explain the observed motion of the cathode spot, or the occurrence of instability only for a narrow range of cathode diameters (see Sec. III B). Additionally, oscillations in a plane observed with ''paddle'' shaped cathodes are not explained by this mechanism.
(3) *Convective.* Convective instabilities can be driven by buoyancy of hot low density gas. The characteristic speeds of buoyancy generated flows are $\sim\sqrt{gL}\sim 0.7$ m/s, where g is the acceleration of gravity and L is a length scale. Since the jet speed in the experiment is ~ 20 m/s,[6] convective effects should not play a role.
(4) *Anode effects.* Effects such as the current distribution in the anode and vapor generation in the anode spot do not explain the dependence of the instability on the cathode geometry.
(5) *''Firehose.''* This type of fluid instability, discussed in Ref. 26 in connection with astrophysical jets, occurs for jets with a confining boundary, such as a hose or a dense surrounding medium. It is also invoked as a destabilizing mechanism in Ref. 15 and to qualitatively explain the arc instability in Ref. 19, with the magnetic field of the arc serving as the confining boundary.
(6) *Current driven.* Current driven ''kink'' instabilities[27] are a strong candidate since such instabilities are known to occur in z pinches, where the geometry is similar to that of the arc.
(7) *Cathode spot motion.* Cathode spot motion is observed in the experiment and can account for the observed arc shape, as will be shown in the following.

The last three possible instability mechanisms appear to be the most likely candidates. Their expected characteristics are compared in Table I, with the experimentally confirmed characteristics in italics.

As can be seen from Table I, a current-driven column and ''firehose''-type instabilities have characteristics that conflict with the experimental observations of the instability. Neither one can explain the occurrence of the instability for only a range of cathode diameters or the linear spatial growth of the arc shape. The cathode spot motion model, on the other hand, is able to account for the observations and is developed in the following. Further discussion of possible mechanisms of instability is given in Sec. VI B. Discussion of the possible causes of the cathode spot motion is deferred until Sec. V.

B. Derivation of arc shape based on the spot motion model

The notion that the cathode spot motion can be an instability mechanism and can influence the shape of the arc column via the cathode jet is mentioned by Bowman.[2] Guillery and Finkelnburg[18] suggest that cathode spot mobility is necessary for the formation of a helical arc shape. However, no quantitative implications of spot motion for the arc shape are found in the literature. This section gives a derivation of the shape of the arc column due to the motion of the cathode spot.

The assumptions used in this model of the unstable arc shape are the same as made in the derivation of arc motion in external magnetic field[6] (single fluid, thin wire, constant jet speed, small amplitude displacement), except for the conditions at the cathode. In that derivation a fixed cathode spot was assumed. Here, the cathode spot is allowed to move over the cathode surface. To simplify the derivation, the cathode surface is assumed to be flat. As before, the cathode jet is assumed to start out normal to the cathode surface. The range of validity of the model is also discussed in Ref. 6, where it is also shown that the aerodynamic drag with the surrounding air is negligible. With the absence of any external magnetic field, and once again neglecting the self magnetic field effects, the force balance equation is

TABLE I. Expected characteristics for a current-driven column instability, firehose instability, and a spot motion instability. The characteristics in italics are confirmed in the experiment.

	Current driven	''Firehose''	Spot motion
Arc length	Stable for short arc	Stable for short arc	*Unstable for all arclengths*
Cathode spot	Stationary	Stationary	*Moving*
Electrode geometry	Independent	Independent	*Dependent on cathode geometry*
Current	*More unstable for higher current*	*More unstable for higher currents (higher jet speeds)*	Depends on spot motion mechanism
Amplitude growth	Exponential	Exponential	*Linear*
Wavelength	Fixed by dispersion relation	Fixed by dispersion relation	*=(jet speed)/(frequency)*

$$\frac{D\mathbf{v}}{dt}=0. \tag{3}$$

Let the z axis be along the equilibrium arc axis, with the positive direction away from the cathode. Let

$$\mathbf{v}=v_0\hat{z}+\tilde{v}_x\hat{x}+\tilde{v}_y\hat{y}, \tag{4}$$

where v_0 is the unperturbed jet speed, and $\tilde{v}_x$ and $\tilde{v}_y$ are the perturbed transverse velocity components. Expanding convective derivatives and linearizing, one gets

$$\frac{D\mathbf{v}}{dt}=\frac{\partial}{\partial t}(\tilde{v}_x\hat{x}+\tilde{v}_y\hat{y})+v_0\frac{\partial}{\partial z}(\tilde{v}_x\hat{x}+\tilde{v}_y\hat{y})=0. \tag{5}$$

As can be seen from Eq. (5), in the linear approximation the equation of motion separates into x and y components. The equation can thus be solved for motion in a plane and the full 3-D shape recovered by adding out-of-the-plane motion at the end. Choosing the y–z plane, expanding $\tilde{v}_y$ as the convective derivative of transverse displacement ξ, and linearizing, we obtain

$$\tilde{v}_y=\frac{\partial\xi}{\partial t}+v_0\frac{\partial\xi}{\partial z}. \tag{6}$$

Substituting Eq. (6) into Eq. (5) and dropping the subscript on v_0,

$$\frac{\partial^2\xi}{\partial t^2}+2v\frac{\partial^2\xi}{\partial t\,\partial z}+v^2\frac{\partial^2\xi}{\partial z^2}=0. \tag{7}$$

Assuming that the cathode surface is flat and that the equilibrium arc axis is normal to it, let the position of the cathode spot in the y–z plane be $y=f(t), z=0$. The initial conditions at the cathode are now a function of time: $\xi(z,t)|_{z=0}=f(t)$ and $(\partial\xi/\partial z)|_{z=0}=0$, the latter condition being due to the jet starting out normal to the cathode surface. Fourier transforming in time and incorporating these initial conditions in the Laplace transform in z, the solution is

$$\xi(z,t)=f\left(t-\frac{z}{v}\right)+\frac{z}{v}f'\left(t-\frac{z}{v}\right). \tag{8}$$

The shape of the arc column is thus determined by the trajectory of the spot on the cathode through the effect of the cathode jet.

If the cathode spot is assumed to gyrate on the cathode at a particular angular frequency ω on an ellipse with major and minor radii of a and b, its trajectory on the flat cathode surface can be parametrized as $a\cos(\omega t)\hat{y}+b\sin(\omega t)\hat{x}$. Its motion in the y–z plane would then be simple harmonic: $f(t)=a\cos(\omega t)$. Using Eq. (8), the arc shape as seen in the y–z plane would be

$$\xi(z,t)=a\left[\cos\left(\omega t-\frac{\omega z}{v}\right)-\frac{z\omega}{v}\sin\left(\omega t-\frac{\omega z}{v}\right)\right]. \tag{9}$$

In the x–z plane, the motion would be 90° out of phase. Combining the two, one obtains the 3-D arc shape:

$$\boldsymbol{\xi}(z,t)=a\left[\cos\left(\omega t-\frac{\omega z}{v}\right)-\frac{z\omega}{v}\sin\left(\omega t-\frac{\omega z}{v}\right)\right]\hat{y}+b\left[\sin\left(\omega t-\frac{\omega z}{v}\right)+\frac{z\omega}{v}\cos\left(\omega t-\frac{\omega z}{v}\right)\right]\hat{x}. \tag{10}$$

An illustration of the arc shape described by Eq. (10) is shown in Fig. 12.

As can be seen in Eq. (10), the arc shape has no dependence on mass density, and is determined by the spot motion amplitude a, the frequency ω, and the average jet velocity v.

Equation (10) can be written in dimensionless form by defining $\zeta\equiv z\omega/v$, $\tau\equiv\omega t$, and $\chi\equiv\xi\omega/v$ as in Ref. 6, as well as $A\equiv a\omega/v$ and $B\equiv b\omega/v$:

$$\boldsymbol{\chi}(\zeta,\tau)=A[\cos(\tau-\zeta)-\zeta\sin(\tau-\zeta)]\hat{y}+B[\sin(\tau-\zeta)+\zeta\cos(\tau-\zeta)]\hat{x}. \tag{11}$$

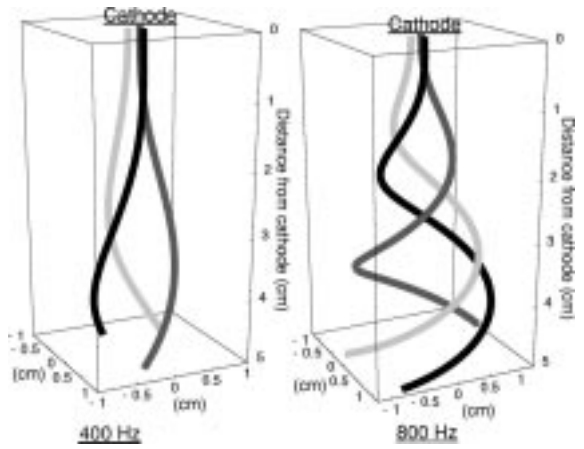

FIG. 12. Derived arc shape [Eq. (10)] for circular gyration of the spot on the cathode for two frequencies of gyration: 400 and 800 Hz. Arc shape is shown at three instances in time with three different shades of gray. Jet speed is 30 m/s; radius of gyration is 1.5 mm. Horizontal scale is expanded.

For short arc lengths, when $\zeta \ll 1$, Eq. (11) can be Taylor expanded:

$$\boldsymbol{\chi}(\zeta,\tau) = A\hat{y}\left[\cos(\tau)\left(1+\frac{\zeta^2}{2}\right)+\frac{\zeta^3}{3}\sin(\tau)\right] + B\hat{x}\left[\sin(\tau)\left(1+\frac{\zeta^2}{2}\right)+\frac{\zeta^3}{3}\cos(\tau)\right]+\mathcal{O}(\zeta)^4. \tag{12}$$

The arc shape for short electrode gaps is thus parabolic with a cubic correction important for the $\hat{y}$ component when phase τ is an odd multiple of $\pi/2$ and for the $\hat{x}$ component when τ is a multiple of π.

As shown in Ref. 23, the model predicts arc length variation at twice the oscillation frequency. Moreover, it has been found experimentally[23] that the arc voltage is proportional to the arc length (the electric field is constant along the arc column at approximately 9 V/cm). Thus harmonic generation on the arc voltage is expected. Depending on whether the spot is moving in a circular or more elongated orbit on the cathode, the amplitude of length variation will change.[23] As discussed in Sec. III A, a harmonic of the oscillation frequency is usually present on the voltage and current wave forms whose strength with respect to the fundamental varies over time. Additional details can be found in Ref. 23.

C. Application of the spot motion model to the instability experiments

Arc instability data are analyzed on the basis of the spot-motion model derived previously. The derived equation for arc shape is fitted to the arc shape obtained from arc images. Since the arc shapes obtained in the experiment are two-dimensional (2-D) projections of what is, in general, a 3-D arc shape, Eq. (9) was used to analyze the 2-D images of the direct view and the 90° mirror view of the arc. There are two free parameters for a 2-D projection of the model: the spot motion amplitude a and the jet velocity v (in 3-D b would be a parameter as well). For a particular measured oscillation frequency ω, the first one determines the amplitude of the arc oscillation, the second—the wavelength.

Since the phase of the spot motion τ is not known from the experiment, it is a fitted parameter as well. A fitted parameter θ has been added to account for any small angle (typically $<5°$) offset of the jet from the electrode axis. This takes into account, for example, any deviation of the cathode endface from the horizontal of the camera's field of view.

The direction of the Earth's magnetic field is transverse to the arc current, which puts a small parabolic deflection bias on the arc column. From the data on arc deflection in a transverse magnetic field,[6] the maximum deflection occurs at the anode, and for the 0.4 G Earth's magnetic field, it is 1 mm for a 4-cm-long arc. This deflection is much smaller than the ≈ 1 cm arc column displacement due to the instability and is neglected in the model.

The arc shape obtained from the camera images has the origin set at the brightest location—the cathode spot. The fit function must therefore be zeroed to the spot location by subtracting $\xi(z=0)=a\cos(\tau)$ from Eq. (9). The form of the equation that is fitted to the arc shape then becomes

$$\xi_{\mathrm{fit}}(z) = a\left[\cos\left(\tau-\frac{\omega z}{v}\right)-\frac{z\omega}{v}\sin\left(\tau-\frac{\omega z}{v}\right)-\cos(\tau)\right]+\theta z, \tag{13}$$

with a, v, τ, and θ as fit parameters.

Since a single frequency of oscillation ω was assumed in deriving Eq. (13), the fits are done for runs where the frequency of oscillation is still distinct, unlike the large amplitude runs such as those of Figs. 6 and 10. Also, because of the additional phase parameter τ, the fits had to be done for arcs sufficiently long or the frequency of oscillation sufficiently high to have at least half a wavelength on the arc column in order to uniquely determine the spot motion amplitude, phase, and the jet speed.

Examples of typical fits using Eq. (13) are shown in Fig. 13. In the majority of cases, good agreement can be seen, with the fit correlation coefficient R generally 0.94 or higher, and typically above 0.98. The example of Fig. 13(c) illustrates a case where a good fit was not obtained. Such column displacements may be due to a nonharmonic displacement of the cathode spot and/or motion of the cathode spot outside the flat cathode tip area assumed in the model.

The amplitudes of spot motion inferred from the fits can be compared to the amplitudes measured from close-up, high resolution images of the cathode region, such as shown in Fig. 11(a). The amplitude was obtained for four runs by finding the center of the luminous arc column immediately below the cathode for each of the 30 images per run, and taking the distance between the extreme left and extreme right positions of the column center as being twice the amplitude of the spot motion. Fig. 14(a) has superimposed on it the four measured amplitudes and the amplitudes inferred from the fits of the model. The plot confirms that the spot motion amplitudes required by the model to describe the observed arc shape are fairly close to those actually present in the

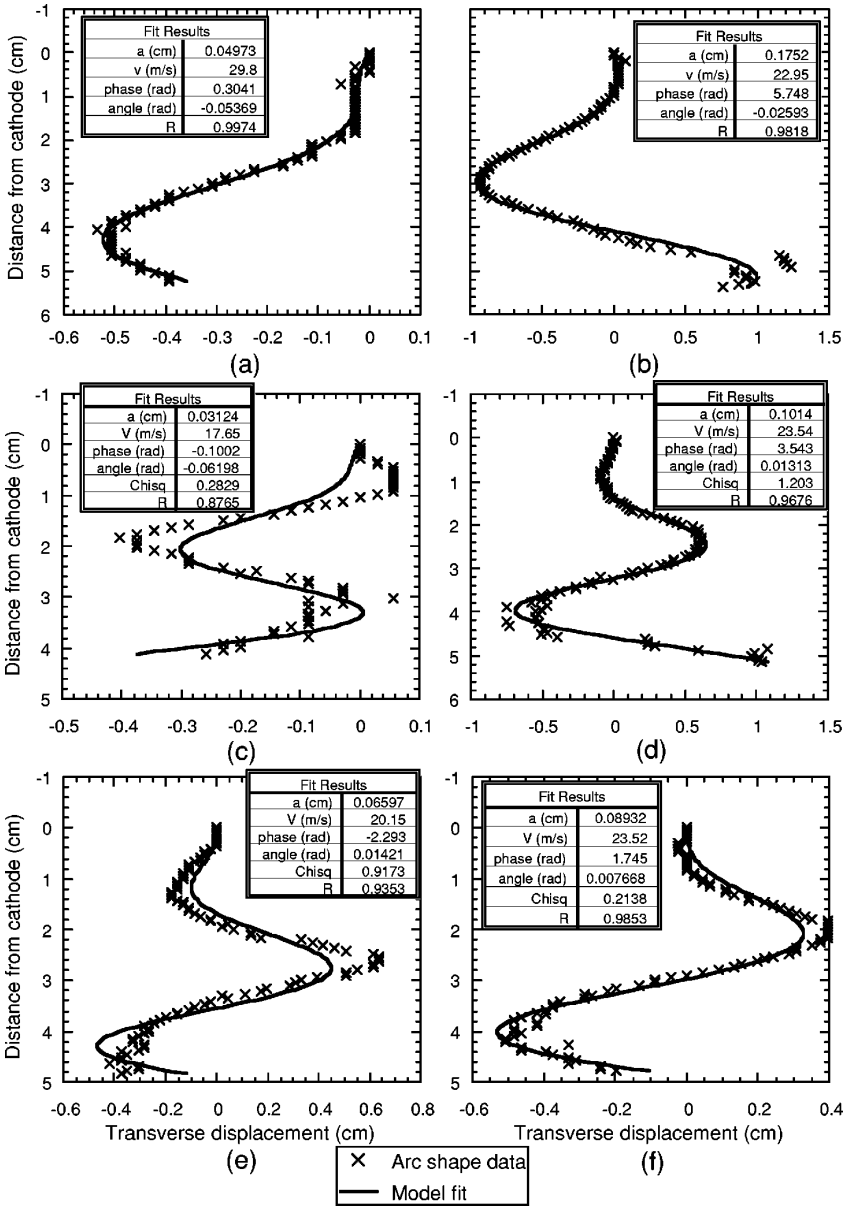

FIG. 13. Examples of fits of the model to the experimentally obtained arc shape during instability. The instantaneous arc current and the frequency of oscillation, respectively, are: (a) 250 A, 575 Hz; (b) 230 A, 520 Hz; (c) 212 A, 650 Hz; (d) 220 A, 780 Hz; (e) 197 A, 650 Hz; (f) 222 A, 600 Hz. In (a)–(c) the data are from the mirror view of the arc; in (d)–(f) from the direct view. Note: the horizontal scales are expanded and are different in each example.

experiments. Fig. 14(b) gives the maximum arc displacement at 4 cm from the cathode as inferred from the fits to arc shape for the same data set.

Figure 15 compares the jet speed inferred from fitting the model to the unstable arc shape to that inferred from the applied transverse magnetic field experiments with the same type of arc, described in Ref. 6. The inferred jet speed increases with the arc current, as expected from Maecker's scaling,[28] and has approximately the same slope as in the applied field experiments. The approximate agreement indicates that the jet speed required for the spot motion model to fit the instability data is consistent with that inferred from the applied field experiments, as expected.

It should be emphasized that this one-dimensional model can only be applied to describe the low amplitude arc column displacements, such as in Fig. 13, and cannot be used to describe the large amplitude displacements such as seen in Fig. 10. It is plausible that these cases do not lie outside the framework of the spot motion model, but require a more sophisticated treatment for quantitative analysis than the one-dimensional approximation used here.

V. POSSIBLE CAUSES FOR CATHODE SPOT MOTION

In Sec. IV a cathode spot motion model of the arc instability was developed and applied to the measured arc column displacement. This section discusses the processes in the

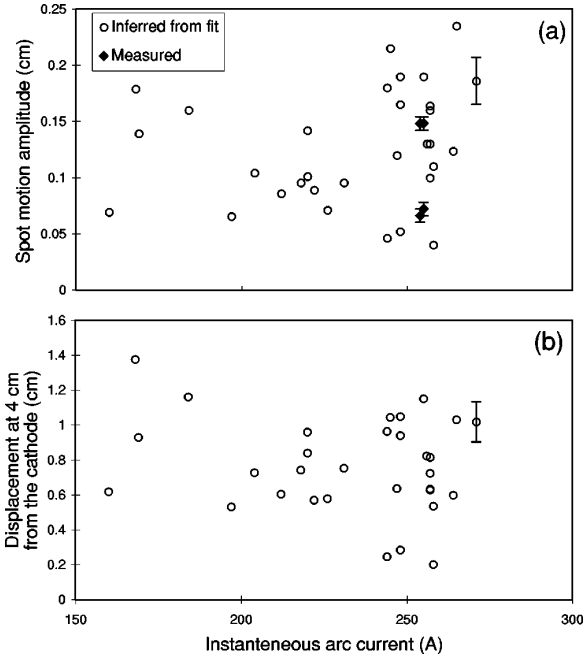

FIG. 14. (a) The spot motion amplitude inferred from the fits of the model to unstable arc shape for instantaneous arc current. Also plotted are the measured amplitudes for four runs. The error bars on the measured amplitudes reflect the image resolution, while the error bars shown on several of the inferred amplitudes are typical standard errors from the fits. (b) Maximum arc displacement at 4 cm from the cathode as inferred from the fits to arc shape for the same data set as in (a). No trend vs current is apparent; however, a trend may be masked by the scatter in spot motion amplitudes due to the data set having been collected over many runs with cathodes at various stages of erosion.

cathode region of the arc, the cathode surface, and the cathode bulk which could be responsible for the motion of the cathode spot itself.

Motion of cathode spots in vacuum arcs and arcs on nonrefractory or ''cold'' cathodes has been has been extensively discussed in the literature (see, e.g., Refs. 29–31, and references therein). However, no comprehensive theory of their spot motion exists. Spot motion on the refractory cathodes, such as carbon, has received less attention and is also not understood.[2] This is probably due to the fact that in the low current arcs, which were studied the most from the basic physics point of view, the cathode spot is fixed or slowly moving.[32]

Section V A discusses the conditions under which the cathode spot may be mobile on refractory cathodes; Sec. V B discusses possible reasons for the spot displacement. However, a definitive quantitative explanation for the observed spot motion has not been found. A discussion of the unresolved issues in identifying the causes of this cathode spot motion is given in Sec. V B.

A. Cathode temperature distribution influence on spot mobility

As discussed in Sec. III A, the cathode geometry, and the cathode tip diameter in particular, have a direct effect on arc stability. This section connects this observation to the cathode spot motion model of instability by considering first how the temperature distribution on the cathode surface can affect the mobility of the spot on the cathode, and then the dependence of the temperature distribution on the cathode geometry.

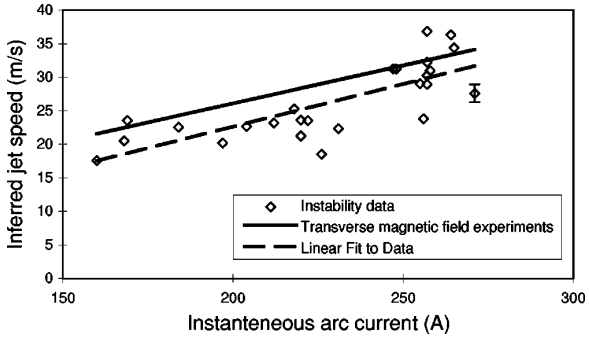

FIG. 15. The jet speed inferred from the fits of the model to the unstable arc shape as compared with the jet speed inferred from the transverse magnetic field experiments—Ref. 6 (solid line) for instantaneous arc current. A least-squares fit to the instability data is also shown. The error bars are typical standard errors from the fits.

The electron emission from graphite cathodes in a high pressure arc for arc currents $\lesssim 1$ kA is governed by thermionic emission.[32] Sufficient electron emission can thus only occur for high surface temperatures (≈ 4000 K). Since the temperature at the cathode spot must remain at ≈ 4000 K, an increase in the heat removal rate from the region adjacent to the cathode spot results in a more peaked, high-gradient temperature distribution. In particular, the rate of heat removal is higher for larger cathode diameter due to increased heat conduction. This is illustrated schematically in Fig. 16(a). Thus, it becomes less likely for the cathode spot to move to a neighboring location for a larger diameter cathode.

For sufficiently small diameter cathodes, on the other hand, the conduction of heat is replaced by radiation from the surface as the dominant mechanism of heat removal out-

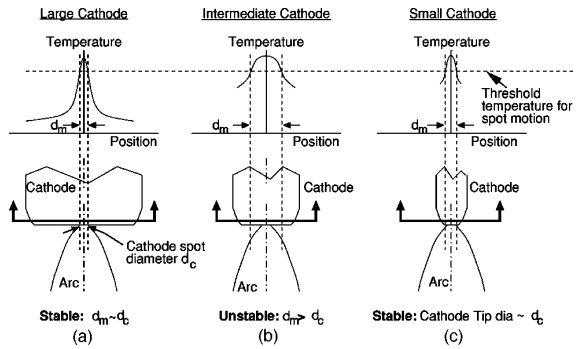

FIG. 16. A schematic illustrating the dependence of the temperature distribution and spot mobility on the end-face of the cathode on the cathode diameter. d_m is the diameter of the region on the cathode surface with sufficient temperature for spot motion; d_c is the cathode spot diameter. (a) Narrow temperature distribution for a large diameter cathode: $d_m \approx d_c$ and the spot is immobile; (b) a wider distribution on a smaller diameter cathode: $d_m > d_c$ and the spot can move; (c) cathode tip diameter $\approx d_c$: the spot is immobile.

side of the cathode spot. In this case, the temperature distribution on the tip of the cathode is wider, anchoring the cathode spot less strongly [Fig. 16(b)]. If the cathode tip diameter is decreased further until it is on the order of the cathode spot diameter, the spot has no room to move, and the arc is once again stabilized. [Fig. 16(c)].

This is a qualitative explanation for the sensitivity of the arc instability to the cathode tip area shown in Fig. 8. In order to quantify this discussion, the cathode radius at which the power conducted into the cathode bulk equals that radiated from the surface can be roughly estimated as follows. The conduction is given by

$$P_{\mathrm{cond}}=\frac{\kappa \Delta T A}{L}\sim \kappa T \pi r, \tag{14}$$

where κ is thermal conductivity, $\Delta T/L$ is the temperature gradient, r is the cathode tip radius, $A\sim\pi r^2$, $L\sim r$, and $\Delta T\sim T$ since the average cathode tip temperature T is much higher than that in the cathode bulk. The radiated power, assuming blackbody radiation, is given by

$$P_{\mathrm{rad}}=(\text{surface area})\,\sigma_S T^4\sim 3\pi r^2 \sigma_S T^4, \tag{15}$$

where σ_S is the Stefan–Boltzmann constant, and the radiating surface area is approximated as the end face of the cathode tip plus the cylindrical side of height r. Equating Eqs. (14) and (15) and solving for r, one obtains

$$\begin{aligned} r\sim \frac{\kappa}{3\sigma_S T^3}&\sim \frac{(30\ \mathrm{W/m\,K})}{3(5.7\times 10^{-8}\ \mathrm{W/m^2\,K^4})(3\times 10^3\ \mathrm{K})^3}\\ &\sim 6\times 10^{-3}\ \mathrm{m}\\ &= 6\ \mathrm{mm}, \end{aligned} \tag{16}$$

where the average tip temperature T was taken to be 3000 K and the value for κ at 3000 K was taken from Ref. 33.

For radii smaller than the above-mentioned estimate, the conducted power decreases, while power radiated increases due to increase in temperature, assuming the input power from the arc remains constant as a function of tip radius. Thus, at half the radius ($r=3$ mm) the conducted power decreases by a factor of 2 while the radiated power increases by a factor of 3/2 via an average tip temperature increase to 3400 K.

In the above discussion, κ was assumed constant. In fact, thermal conductivity of graphite falls rapidly above 3000 K, decreasing from approximately 30 W/m K at 3000 K to 5 W/m K at 3800 K,[33] and making $P_{\mathrm{rad}}\gg P_{\mathrm{cond}}$, and therefore requiring a higher average tip temperature.

Arc current is also a factor in determining the temperature distribution in the cathode. The heat flux into the cathode has been found empirically to increase linearly with arc current (for a tungsten cathode and up to 1 kA current[34]). This leads to an increase in the average surface temperature of the tip, increasing the spot mobility.

From the above-mentioned reasoning an explanation is suggested for the instability observations, in which the arc is unstable only for a range of cathode tip areas (Fig. 8), and for arc currents above 120 A. The upper threshold on the cathode area for instability corresponds to a cathode tip radius of approximately 3 mm, about where the heat removal becomes radiation dominant and the tip temperature distribution is broader, resulting in weaker anchoring of the spot. Sufficient current is also required to maintain a high temperature on the cathode surface surrounding the spot. An example of the effects of the cathode diameter and arc current on the cathode surface temperature distribution is shown in Fig. 17. As can be seen in Fig. 17, the bright area on the cathode is larger in the higher current case (b) and almost nonexistent outside the cathode spot for the large diameter cathode (c).

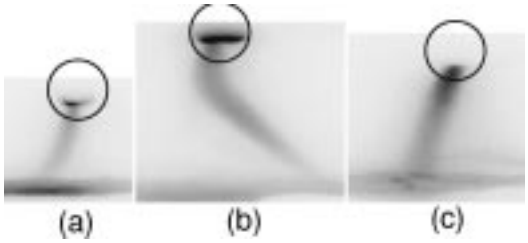

FIG. 17. The brightly glowing high temperature area on the cathode increases for higher arc current and decreases for larger tip diameter (images are negatives, cathode is circled): (a) 3/8-in.-diam cathode at 113 A; (b) 3/8-in-diam cathode at 240 A; (c) 1-in-diam cathode at 253 A (the cathode is too dim to be visible). The arc is stable in (a) and (c) and unstable in (b). The magnification and exposure time are the same for all images; camera gain is the same for (b) and (c) and is 1.5× higher for (a).

Additional support for the hypothesis of cathode temperature distribution affecting stability comes from the ''necked'' cathode run described in Sec. III B. The arc was unstable while it was attached to the wide middle section of the cathode, even though the area of that section exceeded by approximately a factor of 2 the upper threshold area for instability found for solid cylindrical cathodes. In this case, the cathode tip had high thermal resistance despite the large area because the connection to the cathode bulk was only through the narrow (<4.6 mm diam) upper neck. The ''necked'' cathode run, in addition to demonstrating instability dependence on the cathode diameter, also showed that the arc can be unstable on a tip of larger diameter as long as the temperature of the tip can be maintained at a sufficiently high level.

B. Mechanisms of spot motion

The previous discussion gave an indication of the necessary conditions for the cathode spot to be mobile on the cathode, i.e., the spot can only move on a surface of sufficiently high temperature. This section gives possible mechanisms for the spot motion within this region. The mechanisms considered are summarized in Table II and are discussed in the following. As can be seen from Table II, the frequencies expected from current distribution effects in the cathode and cathode vaporization are on the order of those observed experimentally. A rigorous quantitative calculation of the stability of the arc attachment spot at the cathode requires the solution of the full set of time-dependent equations for the energy and particle balance at the cathode–arc interface, as well as for the current and temperature profiles

TABLE II. Possible mechanisms of cathode spot motion. An order of magnitude estimate of the expected frequency of instability for each mechanism is given. Only the last two mechanisms give the expected frequency on the order of the measured one (200–800 Hz). The mechanisms are listed in the order they are discussed in the text.

	Description	Mechanism	Frequency (Hz)
(1)	*Resistive heating in the cathode bulk*	•Ohmic heating under the cathode spot •Resistivity increases with T •Higher voltage in cathode ⇒ Spot shifts to new location	~0.1
(2)	*Surface heating*	•~1 kW heat flux to the cathode surface •Temperature and resistivity rises under cathode spot ⇒ Spot shifts to new location	~0.1
(3)	*Cathode erosion*	•Erosion creates a ''step'' on cathode surface ⇒ Unbalanced entrainment of gas	~0.1
(4)	*Current distribution in the cathode*	(1) Current is constricted in the cathode and in the arc ⇒ A repulsive force ⇒ Unstable equilibrium (2) A force tending to restore the arc current to the electrode axis	~600
(5)	*Vaporization from the cathode spot*	•~1 kW heat flux to the cathode surface •Rapid surface temperature rises leads to vapor production ⇒ Cold resistivity vapor displaces the cathode spot	~500

in the cathode, the cathode sheath, and the adjoining plasma. Because processes occurring in the region, such as electron emission, ion production, cathode heating, and vaporization are all interdependent,[35] solutions to these equations have only been obtained in the literature numerically for steady state while treating the cathode surface as the boundary of the solution region (e.g., Refs. 36–38). In what follows, only orders of magnitude estimates of individual physical mechanisms are attempted.

1. Resistive heating in the cathode bulk

The electrical resistivity of graphite for temperatures above ≈ 1500 K increases linearly with temperature.[39,33] Above a certain critical current density, thermal runaway due to Joule heating in the cathode bulk can take place,[40] causing an increase in the voltage dr op in the cathode and potentially causing spot displacement. The magnitude of this critical current density is estimated[23] on the basis of Ref. 41 to be within a factor of 2 of the current range in the present experiments. However, the time scale for the development of the thermal runaway is found to be ~ 0.8 s.[23] This time scale is much slower than that of the instability time scale ($\sim 2 \times 10^{-3}$ s), and therefore thermal runaway cannot account for the instability.

2. Surface heating

The intense cathode surface heating in the cathode spot also heats the region underneath the cathode spot, increasing resistivity and potentially causing a spot displacement. However, the time scale for the increase to propagate to a depth on the order of the cathode spot radius a is[42] ~ 1.3 s. As with resistive heating, this time scale is much slower than that of the instability time scale.

Both the resistive and surface heating, however, are on the time scale of the slow precession of the cathode spot observed for a stable arc, mentioned in Sec. II. According to the above estimates, the spot would move a spot diameter in ~ 1 s, completing one revolution along the periphery of a 6-mm-diam cathode tip in ~ 10 s. The observed precession period is approximately 20 s. Thermal time scales, therefore, while appearing too slow for the instability, could account for the observation of the slow motion of the cathode spot.

3. Cathode erosion

Measured cathode erosion rates[23] imply an erosion rate per period of oscillation of 1.2×10^{-4} mm. Since this is smaller than the cathode sheath thickness ($\sim 10^{-3}$ mm[32,23]), cathode erosion is too slow to affect spot motion on the instability time scale.

The time scale of the slow precession of the spot on the cathode, however, with a period of ~ 20 s, implies an erosion of ~ 1 mm of cathode material per pass. This can create a geometry with asymmetric entrainment of surrounding gas into the jet, providing the transverse momentum for spot motion.[23] Thus, cathode erosion, in addition to the above-discussed resistivity change, is also a possible mechanism of the observed slow motion of the spot on the cathode.

4. Interaction with the current distribution in the cathode

The resistive diffusion time scale for the graphite cathode is $\sim \mu_0 L^2/\eta \sim 3 \times 10^{-6}$ s, where the length scale L was taken to be the radius of the standard 3/8 in. cathode. Since this is much faster than the time scale of the instability, resistive diffusion does not play a role in the mechanism of the instability and the current distribution in the cathode can be assumed to change instantaneously as the spot is moving on the cathode. Resistivity of the arc plasma (1×10^{-4} Ωm[23]) is higher than that of the graphite cathode, implying an even shorter resistive diffusion time in the arc plasma and no role in the instability mechanism.

Since the diameter of the cathode spot is normally smaller than that of the cathode and that of the arc column, a current constriction exists on both sides of the arc–cathode interface. Any displacement of the cathode spot from the center of a finite-diameter cathode is amplified by the force between the current distributions in the cathode and in the arc, moving the spot toward the edge of the cathode.[23]

On the other hand, the current in the cathode bulk tends to restore the arc current to the electrode axis. Witkowski[19] estimated the frequency of oscillation of the arc column on the basis of this interaction. In his work it was assumed that

the arc is attached at a fixed point on the cathode and that it is the angle of the axis of the arc column with respect to the axis of the cathode that is changing. A simplified analysis led to a harmonic oscillator type differential equation for the angle. The natural frequency of the oscillation is estimated[23] to be ~ 600 Hz, which is in approximate agreement with observed instability frequencies (Sec. III).

However, the assumption of a fixed cathode spot and varying angle does not seem to be justified by observations in the present experiments. The cathode spot is mobile, and although the angle the column makes with the axis of the cathode can vary as is the case in Fig. 10, the column is approximately normal to the cathode surface. Nonetheless, the agreement of the above-mentioned estimate of oscillation frequency with the measured frequency of the instability suggests that electromagnetic interaction may be part of the spot motion mechanism.

5. Cathode vaporization

The high temperatures found in the cathode spot result in vaporization of cathode material.[31] Influx of the carbon vapor with temperature much lower than that of the arc plasma (4000 K vs approximately 12 000 K) would tend to lower the conductivity in the electrode region of the arc and would favor displacement of the arc current to a new location.

Experimental evidence for this effect comes from spectroscopic investigations with a 10 kA copper cathode arc, where a higher temperature plasma was found to rotate around the copper vapor jet.[43] Spectroscopic and photographic studies by Mentel[44] find a cold (4000–5000 K) cathode vapor jet persistent for over 1 cm from the cathode surface for the case of a 1 kA carbon arc. It is furthermore suggested in that paper that the vapor jet tends to displace the cathode spot from the vapor production site.

The frequency of spot rotation on the cathode based on this effect can be estimated as follows. The time scale for the cathode surface to reach sublimation temperature at a new cathode spot location and for vapor production to begin is[42]

$$\tau \sim \frac{\kappa^2 (\Delta T)^2}{q^2 \delta} \sim 5 \times 10^{-4} \text{ s}, \tag{17}$$

where $\kappa \sim 10$ W/m K as before, thermal diffusivity $\delta \sim 1.3 \times 10^{-6}$ m^2/s, $q \sim 2 \times 10^8$ W/m^2 is the energy flux on the cathode surface within the cathode spot diameter, and ΔT is the temperature change need to bring the new location to the sublimation temperature of ≈ 4000 K, and is assumed to be ~ 500 K. If the vapor production time τ is the limiting time scale for the spot displacement, the 2.6-mm-diam cathode spot would complete a revolution around the 6-mm-diam cathode tip in $\sim 1.8 \times 10^{-3}$ s, implying a frequency of ~ 550 Hz, similar to the observed frequencies.

VI. DISCUSSION AND CONCLUSIONS

A. The cathode spot motion model

A systematic study has been conducted of the unstable arc behavior in the 100–250 A current range. A central finding of the experiments is the strong dependence of the instability on the cathode geometry: For the same arc current, the arc is stable or unstable for different cathodes. In particular, for the cylindrical cathodes, the instability occurs only for a relatively narrow range of cathode diameters (Sec. III). The unstable behavior is explained in terms of the cathode spot motion (Sec. IV). The conditions for the spot to be mobile on the cathode are discussed and appear consistent with those seen in the experiments (Sec. V A).

The picture of the ''instability'' that thus emerges is not that of a standard type of exponentially growing instability of, for example, ideal MHD, but is rather a result of periodic motion of the cathode attachment spot on the surface of the cathode. Possible mechanisms for this spot motion were discussed in Sec. V B.

The influence of the self-magnetic field on the arc column remains an open question. Since the arc shape during low amplitude instability is similar to that resulting from an applied time-varying transverse magnetic field,[6] it is expected that the self-field effects would not be dominant in this parameter regime, as discussed in Ref. 6. However, the self-field probably does play a role in the case of large curvature column displacements. For example, although the large displacement of the column in Fig. 10 can be explained qualitatively by the large amplitude spot motion on the curved, wide cathode tip, the self-magnetic field probably plays some role in accentuating the bending.

The occurrence of instability for only a range of cathode diameters is interpreted using the cathode spot motion model as follows. It is argued that due to the temperature dependence of the thermionic emission mechanism, the spot mobility increases for higher and more uniform cathode temperatures. Furthermore, the cathode temperature and temperature uniformity are shown to be higher for smaller cathode diameters. Thus, if the instability is caused by the motion of the spot on the cathode, it will occur for diameters small enough for the spot to be mobile. This diameter is shown to be approximately equal to that observed.

The lower bound on the cathode diameter for instability is interpreted as a physical limit on the excursion of the cathode spot. This lower bound would thus be expected to equal the cathode spot diameter. However, the lower bound diameter is observed to be ≈ 5 mm, still approximately twice the cathode spot diameter at 250 A (≈ 2.6 mm[45]). This may be an indication that the mechanism driving the spot motion ceases to apply below this diameter, even though the spot still has room to move, or that the spot size increased to cover the cathode end-surface.

The mechanism of cathode spot motion remains open (see Sec. V B). Two of the candidates, thermal effects in the cathode and cathode erosion, although both potentially able to produce spot motion, are too slow for time scales of the instability. On the other hand, they do appear to be relevant for the slow precession of the cathode spot. The most likely causes of rapid spot motion are current distribution effects in the cathode and cathode vaporization. However, although these two mechanisms give the correct time scale for the instability, an explanation of how these mechanisms would result in the remarkable regularity of the arc motion over many cycles awaits a more comprehensive theory.

B. Other possible models of the instability

The characteristics of the three most likely models of instabilities were summarized in Sec. IV A. The applicability of the cathode spot motion model to the observations was discussed previously. The other two possible candidates are a current-driven ''kink'' and jet-driven ''firehose''-type instabilities. Either one would explain the observed growth of instability amplitude with current: the latter because the jet speed increases with current. However, they are unlikely to be significant in these experiments for the following reasons.

Neither the ''kink'' nor the ''firehose'' instabilities can easily explain the observed occurrence of the instability only for a narrow range of cathode diameters. These instabilities might be triggered by a change in the current density or the jet speed in the arc column. However, if there is any dependence of these quantities on the cathode diameter, it would be expected to be monotonic, and not specific to a narrow range. Moreover, the influence of the cathode geometry on the unstable arc shape, such as seen in the examples of motion in one plane with the ''paddle''-shaped cathodes, is not explained by these instabilities.

Both a ''kink'' and a ''firehose'' instability would be expected to have exponential growth in time and therefore with distance from the cathode, since the plasma is streaming away from the cathode at the jet speed. In the experiments, linear growth is observed, consistent with the cathode spot motion model. Finally, it is expected that both the ''kink'' and the ''firehose'' modes would be stable for short arcs, when the transit time of the jet across the electrode gap is shorter than the growth time of the instability, whereas the arc is unstable for all lengths studied.

Future work on this instability should include detailed measurements in the cathode region, such as of the cathode temperature distribution and cathode spot size. A direct experimental verification of the thermal nature of the observed stability dependence on the cathode diameter would also be desirable. This could be accomplished by heating or cooling the cathode by external means. Comprehensive modeling of the arc plasma–cathode interaction should be made to resolve the mechanism of the cathode spot motion, including the effects of cathode vaporization and the current distribution in the cathode. Finally, relevance of cathode spot motion to instabilities in industrial arc furnaces could be explored on an intermediate-scale ($\sim$10 kA) experiment.

ACKNOWLEDGMENTS

The authors express thanks for support from Dale Meade, Lewis Meixler, and Ken Young, loan of the Los Alamos National Lab camera from Glen Wurden, technical support from Tom Holoman and Richard Yager, help with German literature from M. Bitter and S. von Goeler, and assistance from A. L. Roquemore and O. Dosunmu. Technical discussions with P. Bellan, G. Bendszak, Ben Bowman, J. Heberlein, S.-E. Stenkvist, and Leonid Zakharov are gratefully acknowledged.

This work was supported by Department of Energy Contract No. DE-AC02-76-CH03073.

[1] P. Fauchais and A. Vardelle, IEEE Trans. Plasma Sci. **25**, 1258 (1997).
[2] B. Bowman, in *Electric Furnace Conference Proceedings, Nashville, TN, 1994* (Iron & Steel Society, Warrendale, 1995), Vol. 52, p. 111.
[3] *The Physics of Welding*, 2nd ed., edited by J. F. Lancaster (Pergamon, New York, 1986).
[4] M. Sharifi, Master's thesis, University of Toronto, 1994.
[5] T. S. Key and D. J. Nastasi, in *Electric Furnace Conference Proceedings, Dallas, TX, 1996* (Iron & Steel Society, Warrendale, 1997), Vol. 54, p. 285.
[6] M. Karasik, A. L. Roquemore, and S. J. Zweben, Phys. Plasmas **7**, 2715 (2000).
[7] H. G. Hülsmann and J. Mentel, Phys. Fluids **30**, 2266 (1987).
[8] H. G. Hülsmann and J. Mentel, Phys. Fluids **30**, 2274 (1987).
[9] P. J. Gaede, Z. Phys. **255**, 40 (1972).
[10] K. Ragaller, Z. Naturforsch. A **29A**, 556 (1974).
[11] K. A. Ernst and J. Kopainsky, Z. Phys. **265**, 253 (1973).
[12] R. E. Blundell, M. T. C. Fang, and A. Vourdas, IEEE Trans. Plasma Sci. **25**, 852 (1997).
[13] A. M. Howatson and D. R. Topham, J. Phys. D: Appl. Phys. **9**, 1101 (1976).
[14] K. Ragaller, U. Kogelschatz, and W. R. Schneider, Z. Naturforsch. A **28A**, 1321 (1973).
[15] P. M. Bellan and J. W. Higley, IEEE Trans. Plasma Sci. **20**, 1026 (1992).
[16] P. E. King, T. L. Ochs, and A. D. Hartman, J. Appl. Phys. **76**, 2059 (1994).
[17] B. Bowman and G. Jordan, in *IEE Conference on Gas Discharges, London, 1970* (IEE, London, 1970), p. 231.
[18] W. Finkelnburg, *Hochstromkohlebogen* (Springer, Berlin, 1948).
[19] V. S. Witkowski, Z. Angew. Phys. **11**, 135 (1958).
[20] R. W. Montgomery and C. M. H. Sharp, Br. J. Appl. Phys., J. Phys. D **2**, 1345 (1969).
[21] X. Wang, J. Liu, Y. Gong, G. Li, and T. Ma, Phys. Plasmas **4**, 2791 (1997).
[22] S.-E. Stenkvist, Iron Steel Eng. **62**, 50 (1985).
[23] M. Karasik, Ph.D. thesis, Princeton University, 2000.
[24] P. Plaschko, J. Fluid Mech. **92**, 209 (1979).
[25] S. C. Crow and F. H. Champagne, J. Fluid Mech. **48**, 547 (1971).
[26] A. Achterberg, Astron. Astrophys. **114**, 233 (1982).
[27] N. A. Krall and A. W. Trivelpiece, *Principles of Plasma Physics* (San Francisco Press, San Francisco, 1986).
[28] H. Maecker, Z. Phys. **141**, 198 (1955).
[29] *Vacuum Arcs: Theory and Application*, edited by J. M. Lafferty (Wiley, New York, 1980).
[30] I. G. Kesaev, *Katodnye protsessy elektricheskoi dugi* (Nauka, Moscow, 1968).
[31] A. E. Guile, IEE Rev. **118**, 1131 (1971).
[32] E. Pfender, in *Gaseous Electronics*, edited by M. N. Hirsh and H. J. Oskam (Academic, New York, 1978), Vol. I, Chap. 5.
[33] N. S. Rasor and J. D. McClelland, Phys. Chem. Solids **15**, 17 (1960).
[34] M. F. Zhukov, A. C. Koroteev, and B. A. Urukov, *Prikladnaya Dinamika Termicheskoii Plasmy* (Nauka, Novosibirsk, 1975).
[35] G. Ecker, in *Ergebnisse der exakten Naturwissenschaften* (Springer, Berlin, 1961), Vol. 33, pp. 1–104.
[36] T. H. Lee, A. N. Greenwood, and W. D. Breingan, in *Proceedings of the Seventh International Conference on Phenomena in Ionized Gases, Beograd, 1965*, edited by B. Perovic and D. Tosic (Gradevinska Knjiga, Beograd, 1966), Vol. 1, p. 670.
[37] J. W. McKelliget and J. Szekely, J. Phys. D: Appl. Phys. **16**, 1007 (1983).
[38] J. J. Lowke, P. Kovitya, and H. P. Schmidt, J. Phys. D: Appl. Phys. **25**, 1600 (1992).
[39] C. L. Mantell, *Carbon and Graphite Handbook* (Interscience, New York, 1968).
[40] G. Ecker, in *Vacuum Arcs: Theory and Application*, edited by J. M. Lafferty (Wiley, New York, 1980), Chap. 7.
[41] E. Hantzsche, IEEE Trans. Plasma Sci. **PS-11**, 115 (1983).
[42] B. Gebhart, *Heat Transfer*, 2nd ed. (McGraw-Hill, New York, 1971).
[43] G. R. Jones, *High Pressure Arcs in Industrial Devices: Diagnostic and Monitoring Techniques* (Cambridge University Press, Cambridge, 1988), p. 177.
[44] J. Mentel, Appl. Phys. **15**, 179 (1978).
[45] V. P. Guillery, Z. Naturforsch. A **10A**, 248 (1955).